



# Ultrasonic-assisted spray pyrolysis technique for synthesis of transparent S-doped TiO<sub>2</sub> thin film

Ghader Hosseinzadeh<sup>1</sup> · Hossein Rasoulnezhad<sup>2</sup> · Naser Ghasemian<sup>1</sup> · Reza Hosseinzadeh<sup>3</sup>

Received: 22 February 2018 / Revised: 23 July 2018 / Accepted: 23 July 2018 / Published online: 31 July 2018  
© Australian Ceramic Society 2018

## Abstract

Nanostructured TiO<sub>2</sub> and S-doped TiO<sub>2</sub> thin films with high transparency were prepared on glass substrate through ultrasonic-assisted spray pyrolysis technique. The effect of sulfur doping on morphological, optical, and structural properties of TiO<sub>2</sub> was studied by scanning electron microscopy (SEM), X-ray diffraction (XRD), Raman spectroscopy, FTIR, photoluminescence spectroscopy, and UV–visible absorption spectroscopy techniques. Because of the high uniformity and monodispersity of the prepared TiO<sub>2</sub> and S-doped TiO<sub>2</sub> thin films, these samples have high visible-light transparency of about 81.89% and 69.73%, respectively. Both the TiO<sub>2</sub> and S-doped TiO<sub>2</sub> thin films have anatase crystal structure; however, introduction of the S dopant in the lattice of TiO<sub>2</sub> creates some oxygen vacancies and structural defects in the S-doped TiO<sub>2</sub> sample. Because of the presence of defects which could act as charge trapping center in the structure of S-doped TiO<sub>2</sub>, this sample has lower electron–hole recombination rate than undoped TiO<sub>2</sub>. Furthermore, sulfur doping results in the band-gap narrowing of TiO<sub>2</sub>. Compared to the undoped TiO<sub>2</sub> sample, suppression of the electron–hole recombination and band-gap narrowing in the S-doped TiO<sub>2</sub> thin film result in the enhancement of its visible-light photocatalytic activity.

**Keywords** S doping · Titanium dioxide · Transparent · Ultrasonic · Spray pyrolysis

## Introduction

Presence of organic dyes in industrial and textile wastewaters has raised significant environmental concerns. Furthermore, water pollution with organic dyes is a serious threat to the living organisms because of their toxicity and carcinogenic nature. Currently available methods for water treatment from dye pollutants are microbial degradation [1], photocatalytic degradation [2], adsorption [3, 4], advanced oxidation [5], filtration [6, 7], and sonolysis [8]. Among these methods, photocatalytic degradation is the most effective and simple

approach for cleaning of organic dyes from polluted water and wastewater.

Among the various semiconductor photocatalysts like WO<sub>3</sub>, ZnWO<sub>4</sub>, ZnO, and BiTiO<sub>3</sub> [9–11], undoubtedly TiO<sub>2</sub> is the most commonly used one for the photocatalytic degradation of organic contaminants in water owing to its high oxidizing power, non-toxicity, good chemical stability, cheapness, and high photocatalytic activity [12, 13]. The major drawback of TiO<sub>2</sub> is its relatively wide band-gap energy (3.0 to 3.2 eV [14]), which limits its photocatalytic activity to the UV region. Another important factor that has significant effect on the photoactivity of a photocatalyst is the electron–hole recombination rate, and any factor that reduces the electron–hole recombination rate will improve the photocatalytic activity [15]. In this regard, numerous methods like sensitizing with semiconductor quantum dots (QDs) or organic dyes [16, 17], doping and codoping with metal and non-metal elements [18, 19], and compositing with carbon nanomaterials [20, 21] have been developed to improve the visible-light photocatalytic activity of TiO<sub>2</sub>.

In the case of sulfur doping into the TiO<sub>2</sub> crystal lattice, sulfur can present in more than one oxidation state such as S<sup>2-</sup>

✉ Ghader Hosseinzadeh  
g.hosseinzadeh@bonabu.ac.ir

<sup>1</sup> Department of Chemical Engineering, University of Bonab, Bonab, Iran

<sup>2</sup> Department of Electrical & Electronics Engineering, Standard Research Institute (SRI), Karaj, Iran

<sup>3</sup> Medical Laser Research Group, Medical Laser Research Center, ACECR, Tehran, Iran

(anionic), or  $S^{6+}$  (cationic), depending on the synthesis conditions and the precursor type [22]. Furthermore, the elemental S atoms can occupy the substitutional and interstitial sites in the  $TiO_2$  lattice and the mixing of S 3p states with valence band of  $TiO_2$  can cause the band-gap energy to decrease [23]. For these reasons, preparation of S-doped  $TiO_2$ , for photocatalytic applications, has attracted increasing attention in recent years [24].

To avoid the expensive and complex separation of the photocatalyst after degradation processes,  $TiO_2$  in the form of thin film on a substrate are preferred to the  $TiO_2$  nanoparticle suspensions. Semiconductor-based photoactive films are deposited on various substrates of metals, ceramics, silicon wafer, and glass in widespread applications such as solar cells, self-cleaning surfaces, hydrogen production, photocatalysis, and air purification [25]. Among these substrates, glass substrate is the most appropriate because it has excellent chemical stability, high transmittance, and low cost. Transparency is an important requirement in consideration of the potential photocatalytic application of coatings on the building and vehicle glass; for these reasons, there is considerable interest on the preparation of transparent photoactive films on glass substrate [26, 27].

Pure and doped  $TiO_2$  thin films have been prepared by a variety of techniques such as mechanical alloying [28], sputtering [29], sol–gel [30], pulsed laser deposition [31], spray pyrolysis [32], and solvothermal [33] methods. However, these techniques suffer from several limitations like use of toxic organometallic reagents, expensive equipment, complex reaction process, and long reaction time. In the present work, pure and S-doped  $TiO_2$  thin films with high monodispersity and transparency were deposited on glass substrate through a simple design based on ultrasonic-assisted spray pyrolysis technique. The visible-light photocatalytic activity of the prepared samples was evaluated by measuring the degradation of methylene blue (MB) under visible-light radiation.

## Material and methods

### Materials

All chemicals were used without further purification. The following chemicals were used in this work: titanium(IV) butoxide ( $\geq 97.0\%$  from Sigma-Aldrich), thiourea ( $\geq 99.0\%$  from Sigma-Aldrich), concentrated hydrochloric acid (37 wt%, Merck), and absolute ethanol (99.5% v/v, Merck).

### Preparation of $TiO_2$ thin films

The schematic illustration of the thin-film deposition system is shown in Fig. 1. At first,  $TiO_2$  sol solution was prepared by dropwise addition of 30 ml ethanolic solution of HCl (0.01 M) into the 30 ml of ethanolic solution of titanium(IV) butoxide

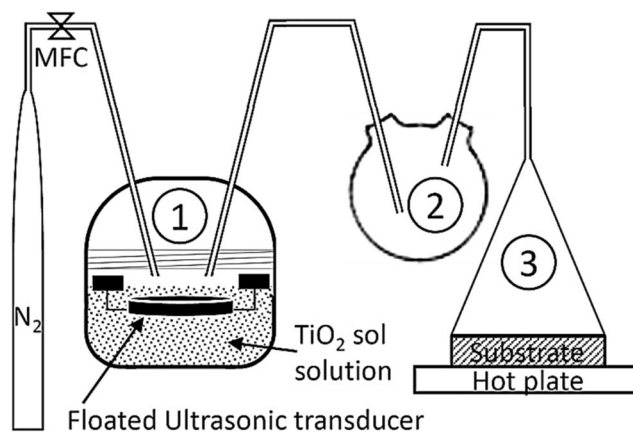


**Fig. 1** Schematic illustration of the ultrasonic-assisted spray pyrolysis technique

(0.71 M). In order to control the hydrolysis of titanium(IV) butoxide precursor, pH of final solution was adjusted to 2.1 by addition of HCl solution (0.01 M). After 2 h of stirring, the obtained solution was poured into flask 1. As Fig. 1 shows, a piezoelectric ultrasonic transducer was floated on the surface of the  $TiO_2$  sol solution, and by generation of ultrasonic waves sprayed the solution as small droplets which were carried by  $N_2$  gas (with a flow rate of 200 ml/min) into flask 2. Inside flask 2, large droplets were separated from the small ones by sedimentation which results in the improving of the monodispersity of the obtained thin films. In flask 3 with collision of the migrated droplets to hot glass substrate (at 400 °C), they are thermally decomposed to form  $TiO_2$  thin film. The deposition time is 30 min. The preparation procedure of S-doped  $TiO_2$  thin films (with 1%wt S) is the same as that of the  $TiO_2$  thin films except that 41 mg thiourea was added into the 30 ml of ethanolic solution of titanium(IV) butoxide (0.71 M).

### Characterization

X-ray diffraction (XRD) patterns of the prepared thin films have been recorded by a STOE Stadi diffractometer equipped with Cu-K $\alpha$  irradiation ( $\lambda = 1.54018 \text{ \AA}$ ). Photoluminescence (PL) emission spectra of the prepared samples were determined using Cary Eclipse fluorescence spectrophotometer (Varian, Inc., USA) at room temperature, with an excitation wavelength of 300 nm. Raman spectra of the samples were obtained using T64000-HORIBA Jobin Yvon Raman spectrometer equipped with an argon ion laser (514 nm). FTIR spectra of the samples were recorded using Bruker V33 spectrometer. The surface morphology and EDS (energy-dispersive X-ray spectroscopy) elemental analysis of the thin films were examined using MIRA3 TESCAN field emission scanning electron microscope (FESEM) (Czech Republic). Ultraviolet–visible (UV–vis) absorption and transmission

spectra of the samples were recorded using Cary 100 Bio spectrophotometer (Varian, Inc., USA).

### Evaluation of the visible-light photocatalytic activity of the thin films

The visible-light photocatalytic activity of the prepared thin film was examined by measuring the photocatalytic degradation of MB (as a model of organic dyes). Five milliliters of the dye solution with an initial concentration of 10  $\mu\text{M}$  was added to a cuvette containing a thin-film sample with an active surface area of 2  $\text{cm}^2$ . Then the cuvette was sealed with glass to prevent solution evaporation. Before irradiation, the reaction solution was stirred in the dark condition for about 12 h to achieve an adsorption–desorption equilibrium. Afterward, a 570-W Xenon lamp (OSRAM Co) as visible-light source was placed at 15 cm from the reaction solution along with L41 UV cutoff filter (Kenko Co.), and the solution was irradiated at room temperature. At given time intervals, the samples were taken out by a syringe and the remaining concentration of the dye was measured using a Cary 100 Bio spectrophotometer (Varian).

## Results and discussion

### Characterization

#### XRD

The crystalline structure of the  $\text{TiO}_2$  and S-doped  $\text{TiO}_2$  thin films was analyzed by X-ray diffraction (XRD) (Fig. 2). In XRD patterns of these samples, the  $2\theta$  peaks located at  $25.3^\circ$ ,  $37.7^\circ$ ,  $47.9^\circ$ ,  $54.1^\circ$ ,  $55.1^\circ$ , and  $62.8^\circ$  are consistent with anatase lattice planes of (101), (004), (200), (105), (211), and (204) respectively (JCPDS card No. 21-1272). Therefore, both the  $\text{TiO}_2$  and S-doped  $\text{TiO}_2$  thin films have anatase crystal structure and presence of S element does not interfere in the crystal structure of  $\text{TiO}_2$ . The  $\text{TiO}_2$  sample shows sharper XRD peaks (indicating a higher crystallinity) than S-doped  $\text{TiO}_2$  thin film, and as shown in inset of Fig. 2, there is a slight shift and broadening in the (101) XRD peak of the S-doped  $\text{TiO}_2$  sample. Presence of sulfur dopant in the lattice of  $\text{TiO}_2$  may disorder the  $\text{TiO}_2$  crystalline structure which results in the defect formation in the S-doped  $\text{TiO}_2$  [34]. The X-ray diffraction patterns of the thin films show the amorphous structure to some extent, which could be related to the amorphous nature of glass substrate or presences of defects and vacancies in the films.

#### Raman spectroscopy

Raman spectroscopy can be used to identify trace amounts of the different crystal phases of  $\text{TiO}_2$  [35]. Figure 3 shows room-temperature Raman spectra of the prepared samples.

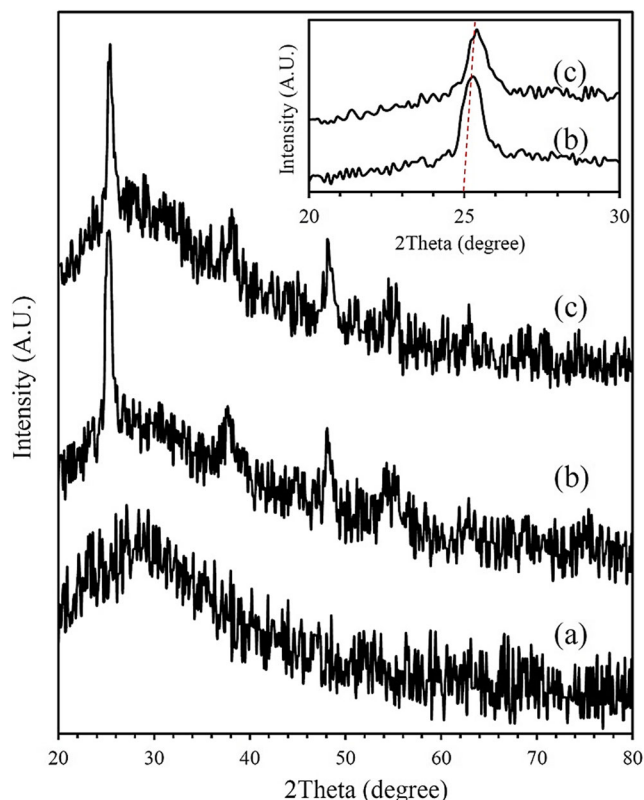


**Fig. 2** XRD patterns of (a) glass substrate, (b)  $\text{TiO}_2$ , and (c) S-doped  $\text{TiO}_2$  thin-film samples

Generally, the anatase  $\text{TiO}_2$  exhibits four major Raman active modes at  $E_g$  ( $144$ ,  $197$ , and  $639\text{ cm}^{-1}$ ),  $B1g$  ( $399\text{ cm}^{-1}$ ), and  $A1g$  ( $519\text{ cm}^{-1}$ ) [36, 37]. In the Raman spectra of  $\text{TiO}_2$  and S-doped  $\text{TiO}_2$  thin films, all of these active modes can be identified, and there is no peak related to rutile phase of  $\text{TiO}_2$ . Hence, anatase is the dominant phase in the prepared thin films. As shown in the inset of Fig. 3, compared to the Raman spectrum of  $\text{TiO}_2$ , in Raman spectrum of S-doped  $\text{TiO}_2$  sample, the peak located at  $144.3\text{ cm}^{-1}$  shifts to  $146.6\text{ cm}^{-1}$ , indicating that introduction of S dopant in the

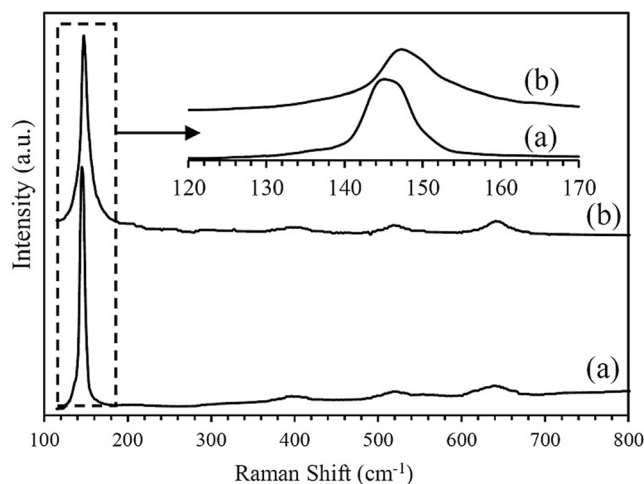


**Fig. 3** Raman spectra of (a)  $\text{TiO}_2$ , and (b) S-doped  $\text{TiO}_2$  thin films

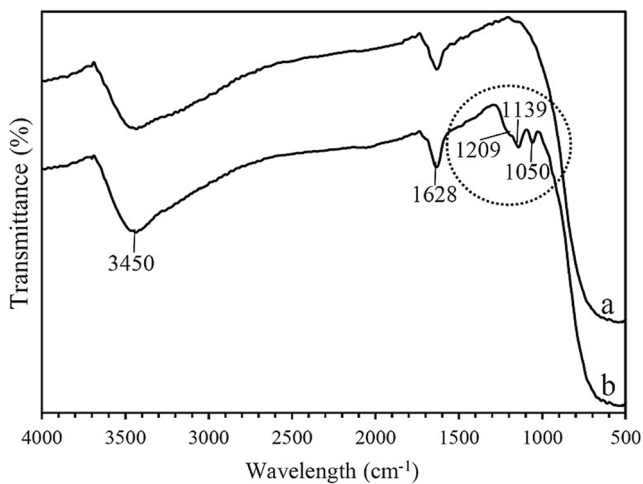


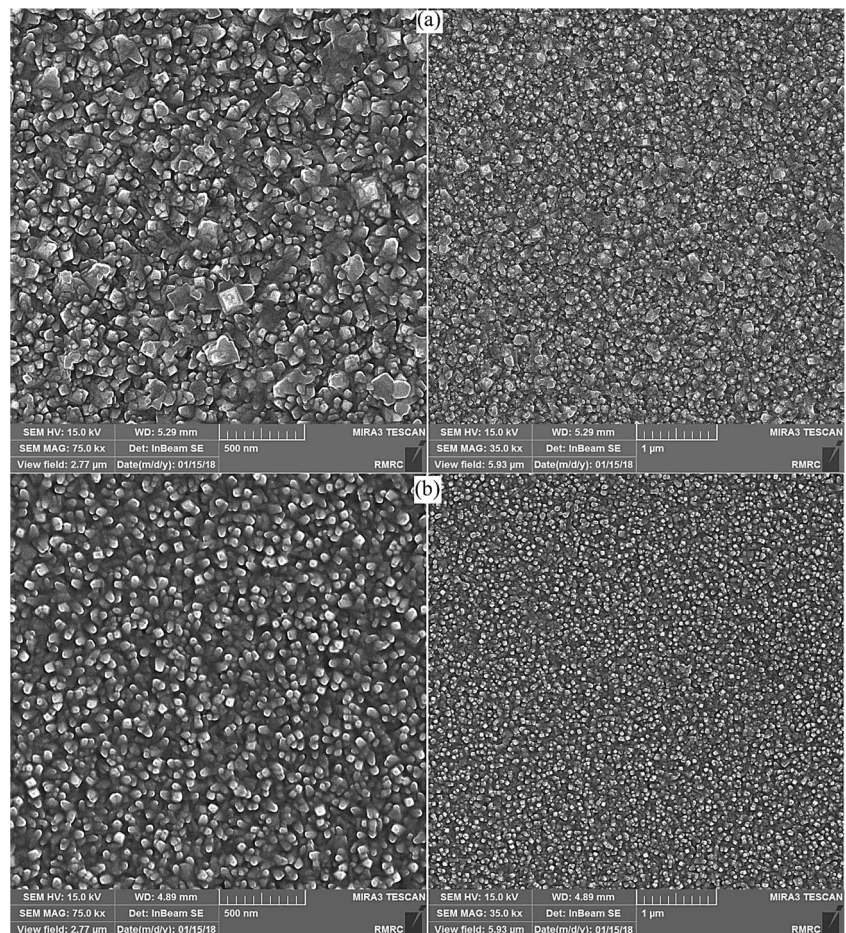
**Fig. 4** FTIR spectra of (a)  $\text{TiO}_2$ , and (b) S-doped  $\text{TiO}_2$  thin films

crystal structure of  $\text{TiO}_2$  increases the number of surface oxygen vacancies and defects [38].

### FTIR

The presences of different functional groups in the synthesized thin films were confirmed from FTIR spectroscopy studies. FTIR

**Fig. 5** FESEM images of **a**  $\text{TiO}_2$ , and **b** S-doped  $\text{TiO}_2$  thin films



spectra of the undoped and S-doped  $\text{TiO}_2$  thin films are presented in Fig. 4. Because of the stretching and bending vibrations of the OH group of the adsorbed water, two obvious peaks at  $3450\text{ cm}^{-1}$  and  $1628\text{ cm}^{-1}$  are observed in FTIR spectra of both  $\text{TiO}_2$  and S-doped  $\text{TiO}_2$  thin films. The broad intense band in the range of  $500\text{--}800\text{ cm}^{-1}$  is due to the vibrations of Ti–O, and O–Ti–O bonds [39]. Compared to the FTIR spectrum of  $\text{TiO}_2$ , three additional absorbance peaks at about  $1050$ ,  $1139$ , and  $1209\text{ cm}^{-1}$  are seen in the FTIR spectrum of S-doped  $\text{TiO}_2$  thin film, which are ascribed to the vibration of S–Ti and Ti–O–S bonds and further confirm the presence of S in the  $\text{TiO}_2$  lattice [37, 40].

### SEM

Surface morphology of the synthesized thin films was characterized by FESEM and Fig. 5 shows FESEM images of the samples at different magnifications. Nanostructures clearly can be seen in the surface of both  $\text{TiO}_2$  and S-doped  $\text{TiO}_2$  thin films. As Fig. 5a indicates, irregular-shaped nanoparticles are observed in the structure of  $\text{TiO}_2$  thin film. However, in the SEM images of the S-doped  $\text{TiO}_2$  thin film (Fig. 5b), semi-cubic nanostructures are present at the surface of this sample, in which the size of these nanostructures is about  $60\text{ nm}$ . Both  $\text{TiO}_2$  and S-doped  $\text{TiO}_2$  thin

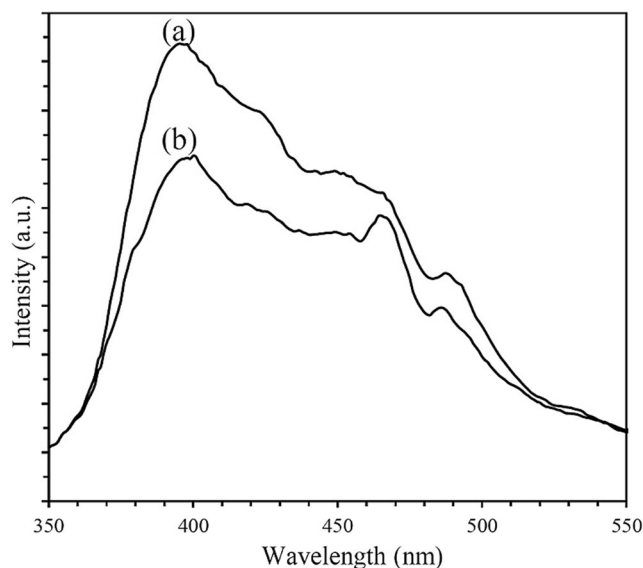
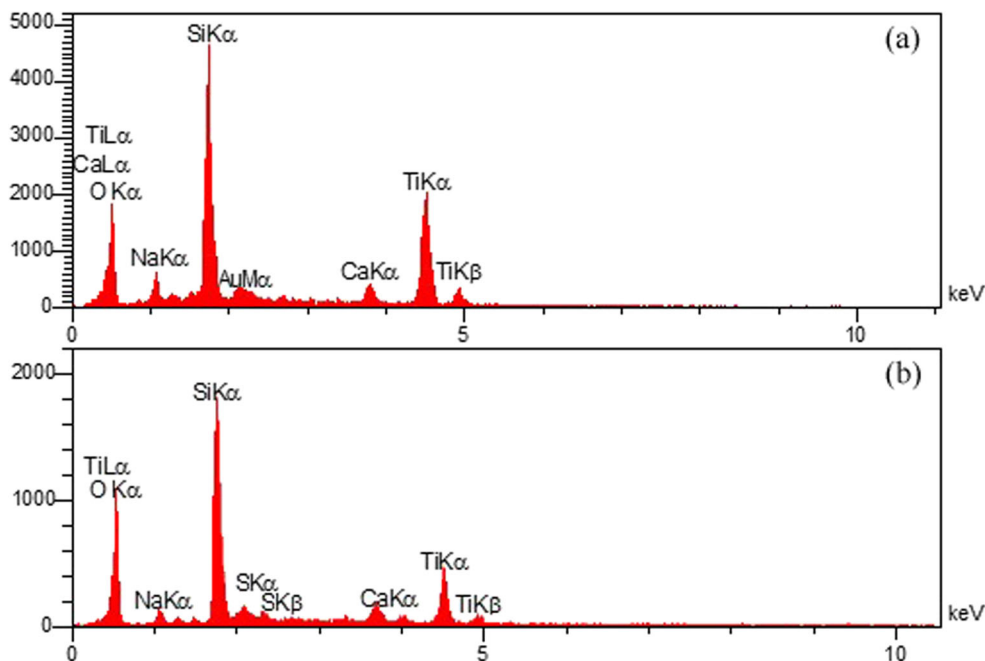
films have high monodispersity and uniformity, and S-doped TiO<sub>2</sub> thin film has higher monodispersity.

Figure 6 indicates EDS spectra of the undoped and S-doped TiO<sub>2</sub> thin films. Besides the peaks related to TiO<sub>2</sub>, the EDS spectra of S-doped TiO<sub>2</sub> thin film displays two additional peaks at about 2.05 and 2.3 keV related to the K $\alpha$  and K $\beta$  lines of S element. Presence of other elements is related to the soda-lime type of glass which was used as substrate.

### Photoluminescence

The photocatalytic activity of the semiconductor photocatalyst greatly depends on the separation and transfer ability for photoinduced electron–hole pairs. For an irradiated semiconductor sample, the photoluminescence (PL) intensity is directly related to the electron–hole recombination rate and the high electron–hole recombination rate results in the high PL intensity, and the low photocatalytic performance [41]. Therefore, the efficiency of charge-carrier trapping in the prepared samples was investigated by PL spectroscopy. As shown in Fig. 7, the S-doped TiO<sub>2</sub> thin film has lower PL intensity than undoped TiO<sub>2</sub> suggesting an enhanced charge transfer and effective separation of electron–hole pairs in S-doped TiO<sub>2</sub>. Both oxygen vacancies and lattice defects in the structure of S-doped TiO<sub>2</sub> can act as charge-carrier trapping centers and thereby decrease the photoinduced electron–hole recombination rate [42, 43]. Therefore, doping of S element reduces the charge-carrier recombination rate and increases the number of photo-generated electrons and holes on TiO<sub>2</sub> surface [44].

**Fig. 6** EDS analysis results of **a** TiO<sub>2</sub>, and **b** S-doped TiO<sub>2</sub> thin-film samples



**Fig. 7** PL spectra of (a) TiO<sub>2</sub>, and (b) S-doped TiO<sub>2</sub> thin-film samples

### Optical properties

Transparency of the prepared thin-film samples was examined via UV–Vis transmittance spectroscopy; the results are shown in Fig. 8. As this figure indicates, in the visible-light region (wavelength of 400–900 nm), the transparency of TiO<sub>2</sub> and S-doped TiO<sub>2</sub> thin films is about 81.89% and 69.73%, respectively. Therefore, because of the high uniformity and monodispersity of the prepared thin films, they have high transparency in the visible-light region.

Figure 9a depicts the UV–visible absorption spectra of the prepared thin films. Compared with undoped TiO<sub>2</sub>, the S-doped TiO<sub>2</sub> thin film has higher visible-light absorbance.

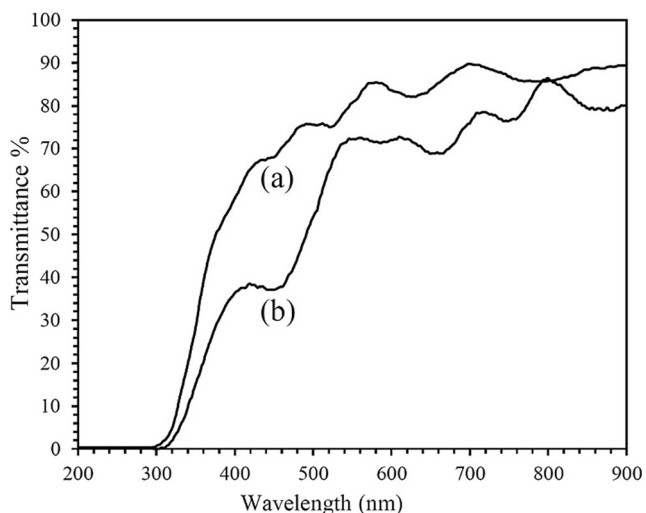


**Fig. 8** Transmittance spectra of (a) TiO<sub>2</sub>, and (b) S-doped TiO<sub>2</sub> thin films

Furthermore, there is a noticeable shift in the absorption edge of the S-doped TiO<sub>2</sub> towards longer wavelengths (red shift), indicating the narrowing of the band-gap energy of TiO<sub>2</sub> by S

doping. The precise value of the band-gap energy ( $E_g$ ) for TiO<sub>2</sub>-based semiconductors can be calculated from the intercept of the tangent line to the plots of  $(\alpha h\nu)^{1/2}$  versus  $h\nu$  (Tauc plots) [45, 46], as shown in Fig. 9b. The estimated band-gap energies of the undoped TiO<sub>2</sub> and S-doped TiO<sub>2</sub> thin films are 3.22 and 2.85 eV, respectively. According to the previous first-principle calculation studies, introduction of S element to the lattice of TiO<sub>2</sub> induces band-gap narrowing by mixing of the S 3p states with the valence band of TiO<sub>2</sub> [47, 48].

### Photocatalytic activity

The visible-light photocatalytic degradation test of MB dye was done to survey the photocatalytic performance of the prepared samples. As Fig. 9c indicates, the visible-light degradation of MB in the absence of any thin-film photocatalyst is negligible; however, in the presence of prepared thin films, there are noticeable improvement in degradation of MB, and photocatalytic activity of S-doped TiO<sub>2</sub> thin film is higher than that of pure TiO<sub>2</sub>. The kinetics of degradation of MB

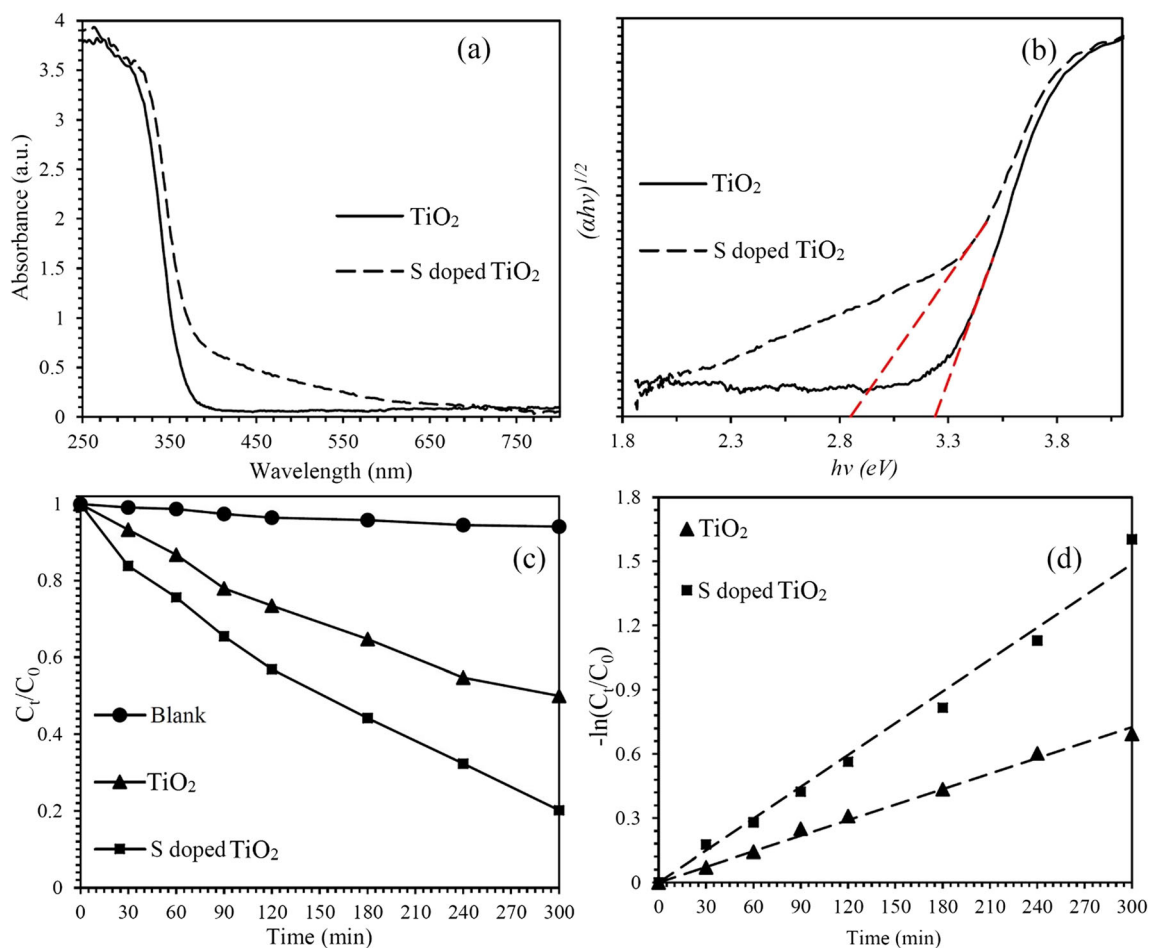


**Fig. 9** **a** UV-Vis absorption spectra, **b** band-gap energy calculation (Tauc plot) of the prepared thin films, **c** the plots of  $C_t/C_0$  versus irradiation time for photocatalytic degradation rates of MB, and **d** calculation of the

corresponding reaction rate constants ( $k$ ) for TiO<sub>2</sub> and S-doped TiO<sub>2</sub> thin films under visible-light irradiation

dye in the presences of the prepared thin films were modeled using the Langmuir–Hinshelwood (L-H) model. For low concentrations of MB, the pseudo-first-order kinetic model can be used for calculation of the reaction rate constants ( $k$ ), represented by Eq. (1) [49]:

$$-\ln\left(\frac{C_t}{C_0}\right) = kt \quad (1)$$

The value of the reaction rate constants ( $k$ ) for visible-light photocatalytic degradation of MB over TiO<sub>2</sub> and S-doped TiO<sub>2</sub> thin films can be estimated from the slope of  $-\ln\left(\frac{C_t}{C_0}\right)$  versus irradiation time ( $t$ ) plots, which Fig. 9d shows these plots. The estimated reaction rate constants for visible-light photocatalytic degradation of MB on TiO<sub>2</sub> and S-doped TiO<sub>2</sub> thin films are 0.0024 and 0.0055 min<sup>-1</sup>, respectively. The low recombination rate of the photoinduced electron–hole pairs and the low band-gap energy of the S-doped TiO<sub>2</sub> thin film may be the reasons for the enhancement of its visible-light photocatalytic activity.

## Conclusion

In summary, at the present work, nanostructured TiO<sub>2</sub> and S-doped TiO<sub>2</sub> thin films with high transparency were deposited on glass substrate through ultrasonic-assisted spray pyrolysis technique. The prepared films were used for the visible-light photocatalytic degradation of MB dye. Both the undoped and S-doped TiO<sub>2</sub> have anatase crystal structure; however, there are some defect and oxygen vacancies in the S-doped sample. Based on the PL spectroscopy results, because of the defect formation in the S-doped TiO<sub>2</sub> thin film, this sample has lower electron–hole recombination rate than TiO<sub>2</sub> thin film. Furthermore, the presence of S dopants in the structure of TiO<sub>2</sub> results in the narrowing of the band-gap energy of TiO<sub>2</sub>. Among the prepared thin films, the S-doped TiO<sub>2</sub> thin film has higher photocatalytic activity than pure TiO<sub>2</sub> sample for the visible-light photocatalytic degradation of MB dye.

## References

- Chen, M., Qin, X., Zeng, G.: Single-walled carbon nanotube release affects the microbial enzyme-catalyzed oxidation processes of organic pollutants and lignin model compounds in nature. *Chemosphere*. **163**, 217–226 (2016)
- Liang, Y., Chen, Z., Yao, W., Wang, P., Yu, S., Wang, X.: Decorating of Ag and CuO on Cu nanoparticles for enhanced high catalytic activity to the degradation of organic pollutants. *Langmuir*. **33**, 7606–7614 (2017)
- Lv, X., Zhao, M., Chen, Z., Zhang, J., Tian, X., Ren, X., Mei, X.: Prepare porous silica nanospheres for water sustainability: high efficient and recyclable adsorbent for cationic organic dyes. *Colloid Polym. Sci.* 1–12 (2018)
- Faghihi, A., Vakili, M.H., Hosseinzadeh, G., Farhadian, M., Jafari, Z.: Synthesis and application of recyclable magnetic freeze-dried graphene oxide nanocomposite as a high capacity adsorbent for cationic dye adsorption. *Desalin. Water Treat.* **57**, 22655–22670 (2016)
- Xie, P., Guo, Y., Chen, Y., Wang, Z., Shang, R., Wang, S., Ding, J., Wan, Y., Jiang, W., Ma, J.: Application of a novel advanced oxidation process using sulfite and zero-valent iron in treatment of organic pollutants. *Chem. Eng. J.* **314**, 240–248 (2017)
- Ting, H., Chi, H.-Y., Lam, C.H., Chan, K.-Y., Kang, D.-Y.: High-permeance metal–organic framework-based membrane adsorber for the removal of dye molecules in aqueous phase. *Environ. Sci. Nano.* **4**, 2205–2214 (2017)
- Kebria, M.R.S., Jahanshahi, M., Rahimpour, A.: SiO<sub>2</sub> modified polyethyleneimine-based nanofiltration membranes for dye removal from aqueous and organic solutions. *Desalination*. **367**, 255–264 (2015)
- Chowdhury, P., Viraraghavan, T.: Sonochemical degradation of chlorinated organic compounds, phenolic compounds and organic dyes—a review. *Sci. Total Environ.* **407**, 2474–2492 (2009)
- Farhadian, M., Sangpour, P., Hosseinzadeh, G.: Preparation and photocatalytic activity of WO<sub>3</sub>–MWCNT nanocomposite for degradation of naphthalene under visible light irradiation. *RSC Adv.* **6**, 39063–39073 (2016)
- Liu, S.-Q.: Magnetic semiconductor nano-photocatalysts for the degradation of organic pollutants. *Environ. Chem. Lett.* **10**, 209–216 (2012)
- Mills, A., Davies, R.H., Worsley, D.: Water purification by semiconductor photocatalysis. *Chem. Soc. Rev.* **22**, 417–425 (1993)
- Chen, X., Mao, S.S.: Titanium dioxide nanomaterials: synthesis, properties, modifications, and applications. *Chem. Rev.* **107**, 2891–2959 (2007)
- Devi, L.G., Kavitha, R.: A review on non metal ion doped titania for the photocatalytic degradation of organic pollutants under UV/solar light: role of photogenerated charge carrier dynamics in enhancing the activity. *Appl. Catal. B Environ.* **140**, 559–587 (2013)
- Landmann, M., Rauls, E., Schmidt, W.: The electronic structure and optical response of rutile, anatase and brookite TiO<sub>2</sub>. *J. Phys. Condens. Matter.* **24**, 195503 (2012)
- Ohtani, B.: Titania photocatalysis beyond recombination: a critical review. *Catalysts*. **3**, 942–953 (2013)
- Sun, W.-T., Yu, Y., Pan, H.-Y., Gao, X.-F., Chen, Q., Peng, L.-M.: CdS quantum dots sensitized TiO<sub>2</sub> nanotube-array photoelectrodes. *J. Am. Chem. Soc.* **130**, 1124–1125 (2008)
- Keihan, A.H., Rasoulnezhad, H., Mohammadgholi, A., Sajjadi, S., Hosseinzadeh, R., Farhadian, M., Hosseinzadeh, G.: Pd nanoparticle loaded TiO<sub>2</sub> semiconductor for photocatalytic degradation of Paraoxon pesticide under visible-light irradiation. *J. Mater. Sci. Mater. Electron.* **28**, 16718–16727 (2017)
- Bakar, S.A., Ribeiro, C.: Nitrogen-doped titanium dioxide: an overview of material design and dimensionality effect over modern applications. *J. Photochem Photobiol C: Photochem Rev.* **27**, 1–29 (2016)
- Bakar, S.A., Byzynski, G., Ribeiro, C.: Synergistic effect on the photocatalytic activity of N-doped TiO<sub>2</sub> nanorods synthesised by novel route with exposed (110) facet. *J. Alloys Compd.* **666**, 38–49 (2016)
- Keihan, A.H., Hosseinzadeh, R., Farhadian, M., Kooshki, H., Hosseinzadeh, G.: Solvothermal preparation of Ag nanoparticle and graphene co-loaded TiO<sub>2</sub> for the photocatalytic degradation of paraoxon pesticide under visible light irradiation. *RSC Adv.* **6**, 83673–83687 (2016)
- Safajou, H., Khojasteh, H., Salavati-Niasari, M., Mortazavi-Derazkola, S.: Enhanced photocatalytic degradation of dyes over

- graphene/Pd/TiO<sub>2</sub> nanocomposites: TiO<sub>2</sub> nanowires versus TiO<sub>2</sub> nanoparticles. *J. Colloid Interface Sci.* **498**, 423–432 (2017)
22. Bakar, S.A., Ribeiro, C.: A comparative run for visible-light-driven photocatalytic activity of anionic and cationic S-doped TiO<sub>2</sub> photocatalysts: a case study of possible sulfur doping through chemical protocol. *J. Mol. Catal. A Chem.* **421**, 1–15 (2016)
  23. Ramacharyulu, P., Kumar, J.P., Prasad, G., Sreedhar, B.: Sulphur doped nano TiO<sub>2</sub>: synthesis, characterization and photocatalytic degradation of a toxic chemical in presence of sunlight. *Mater. Chem. Phys.* **148**, 692–698 (2014)
  24. Bakar, S.A., Ribeiro, C.: Rapid and morphology controlled synthesis of anionic S-doped TiO<sub>2</sub> photocatalysts for the visible-light-driven photodegradation of organic pollutants. *RSC Adv.* **6**, 36516–36527 (2016)
  25. Tsay, C.-Y., Liang, S.-C.: Ultraviolet-assisted annealing for low-temperature solution-processed p-type gallium tin oxide (GTO) transparent semiconductor thin films. *Mater. Sci. Semicond. Process.* **71**, 441–446 (2017)
  26. Pat S, Yudar HH, Korkmaz Ş, Özen S, Mohammadigharehbagh R, Pat Z (2017) Transparent nano layered Li<sub>3</sub>PO<sub>4</sub> coatings on bare and ITO coated glass by thermionic vacuum arc method. *Journal of Materials Science: Materials in Electronics*:1–7
  27. Choi, T., Kim, J.-S., Kim, J.H.: Transparent nitrogen doped TiO<sub>2</sub>/WO<sub>3</sub> composite films for self-cleaning glass applications with improved photodegradation activity. *Adv. Powder Technol.* **27**, 347–353 (2016)
  28. Jho, J.H., Kim, D.H., Kim, S.-J., Lee, K.S.: Synthesis and photocatalytic property of a mixture of anatase and rutile TiO<sub>2</sub> doped with Fe by mechanical alloying process. *J. Alloys Compd.* **459**, 386–389 (2008)
  29. Peng, S., Yang, Y., Li, G., Jiang, J., Jin, K., Yao, T., Zhang, K., Cao, X., Wang, Y., Xu, G.: Effect of N<sub>2</sub> flow rate on the properties of N doped TiO<sub>2</sub> films deposited by DC coupled RF magnetron sputtering. *J. Alloys Compd.* **678**, 355–359 (2016)
  30. Mamane, H., Horovitz, I., Lozzi, L., Di Camillo, D., Avisar, D.: The role of physical and operational parameters in photocatalysis by N-doped TiO<sub>2</sub> sol–gel thin films. *Chem. Eng. J.* **257**, 159–169 (2014)
  31. Ruzybayev, I., Shah, S.I.: The role of oxygen pressure in nitrogen and carbon co-doped TiO<sub>2</sub> thin films prepared by pulsed laser deposition method. *Surf. Coat. Technol.* **241**, 148–153 (2014)
  32. Ravidhas, C., Anitha, B., Raj, A.M.E., Ravichandran, K., Girisun, T.S., Mahalakshmi, K., Saravanakumar, K., Sanjeeviraja, C.: Effect of nitrogen doped titanium dioxide (N-TiO<sub>2</sub>) thin films by jet nebulizer spray technique suitable for photoconductive study. *J. Mater. Sci. Mater. Electron.* **26**, 3573–3582 (2015)
  33. He, Z., Que, W., He, Y., Hu, J., Chen, J., Javed, H.M.A., Ji, Y., Li, X., Fei, D.: Electrochemical behavior and photocatalytic performance of nitrogen-doped TiO<sub>2</sub> nanotubes arrays powders prepared by combining anodization with solvothermal process. *Ceram. Int.* **39**, 5545–5552 (2013)
  34. Lin, Y.-H., Tseng, T.-K., Chu, H.: Photo-catalytic degradation of dimethyl disulfide on S and metal-ions co-doped TiO<sub>2</sub> under visible-light irradiation. *Appl. Catal. A Gen.* **469**, 221–228 (2014)
  35. Tian, F., Zhang, Y., Zhang, J., Pan, C.: Raman spectroscopy: a new approach to measure the percentage of anatase TiO<sub>2</sub> exposed (001) facets. *J. Phys. Chem. C.* **116**, 7515–7519 (2012)
  36. Hsien, Y.-H., Chang, C.-F., Chen, Y.-H., Cheng, S.: Photodegradation of aromatic pollutants in water over TiO<sub>2</sub> supported on molecular sieves. *Appl. Catal. B Environ.* **31**, 241–249 (2001)
  37. Brindha, A., Sivakumar, T.: Visible active N, S co-doped TiO<sub>2</sub>/graphene photocatalysts for the degradation of hazardous dyes. *J. Photochem. Photobiol. A Chem.* **340**, 146–156 (2017)
  38. Li, H., Zhang, X., Huo, Y., Zhu, J.: Supercritical preparation of a highly active S-doped TiO<sub>2</sub> photocatalyst for methylene blue mineralization. *Environ. Sci. Technol.* **41**, 4410–4414 (2007)
  39. Lin, Y.-H., Hsueh, H.-T., Chang, C.-W., Chu, H.: The visible light-driven photodegradation of dimethyl sulfide on S-doped TiO<sub>2</sub>: characterization, kinetics, and reaction pathways. *Appl. Catal. B Environ.* **199**, 1–10 (2016)
  40. Arman, S., Omidvar, H., Tabaian, S., Sajjadnejad, M., Fouladvand, S., Afshar, S.: Evaluation of nanostructured S-doped TiO<sub>2</sub> thin films and their photoelectrochemical application as photoanode for corrosion protection of 304 stainless steel. *Surf. Coat. Technol.* **251**, 162–169 (2014)
  41. Liqiang, J., Yichun, Q., Baiqi, W., Shudan, L., Baojiang, J., Libin, Y., Wei, F., Honggang, F., Jiazhong, S.: Review of photoluminescence performance of nano-sized semiconductor materials and its relationships with photocatalytic activity. *Sol. Energy Mater. Sol. Cells.* **90**, 1773–1787 (2006)
  42. Gritsenko, V.A., Islamov, D.R., Perevalov, T.V., Aliev, V.S., Yelisseyev, A.P., Lomonova, E.E., Pustovarov, V.A., Chin, A.: Oxygen vacancy in hafnia as a blue luminescence center and a trap of charge carriers. *J. Phys. Chem. C.* **120**, 19980–19986 (2016)
  43. Kim, T., Hur, J., Jeon, S.: The influence of interfacial defects on fast charge trapping in nanocrystalline oxide-semiconductor thin film transistors. *Semicond. Sci. Technol.* **31**, 055014 (2016)
  44. Shang, X., Zhang, M., Wang, X., Yang, Y.: Sulphur, nitrogen-doped TiO<sub>2</sub>/graphene oxide composites as a high performance photocatalyst. *J. Exp. Nanosci.* **9**, 749–761 (2014)
  45. Tauc, J.: Absorption edge and internal electric fields in amorphous semiconductors. *Mater. Res. Bull.* **5**, 721–729 (1970)
  46. Wu, G., Nishikawa, T., Ohtani, B., Chen, A.: Synthesis and characterization of carbon-doped TiO<sub>2</sub> nanostructures with enhanced visible light response. *Chem. Mater.* **19**, 4530–4537 (2007)
  47. Yang, K., Dai, Y., Huang, B.: Understanding photocatalytic activity of S-and P-doped TiO<sub>2</sub> under visible light from first-principles. *J. Phys. Chem. C.* **111**, 18985–18994 (2007)
  48. Liu, R., Zhou, X., Yang, F., Yu, Y.: Combination study of DFT calculation and experiment for photocatalytic properties of S-doped anatase TiO<sub>2</sub>. *Appl. Surf. Sci.* **319**, 50–59 (2014)
  49. Alvarez-Corena, J.R., Bergendahl, J.A., Hart, F.L.: Advanced oxidation of five contaminants in water by UV/TiO<sub>2</sub>: reaction kinetics and byproducts identification. *J. Environ. Manag.* **181**, 544–551 (2016)